Modelling the quasi-static behaviour of bituminous material using a cohesive zone model

Amir Tabaković[1], Aleksandar Karač[2], Alojz Ivanković[2], Amanda Gibney[1], Ciaran McNally[1] and Michael D Gilchrist [2*]

[*] corresponding author; michael.gilchrist@ucd.ie

[1] UCD School of Architecture, Landscape and Civil Engineering

[2] UCD School of Electrical, Electronic and Mechanical Engineering

Abstract: This paper investigates the applicability of a cohesive zone model for simulating the performance of bituminous material subjected to quasistatic loading. The Dugdale traction law was implemented within a finite volume code in order to simulate the binder course mortar material response when subjected to indirect tensile loading. A uniaxial tensile test and a three-point bend test were employed to determine initial stress-strain curves at different test rates and the cohesive zone parameters (specifically, fracture energy and cohesive strength). Numerical results agree well with the experimental data up to the peak load and onset of fracture, demonstrating the value of the cohesive zone modelling technique in successfully predicting fracture initiation and maximum material strength.

Key words: Binder course mortar, finite volume method, indirect tensile loading, three-point bend test.

Nomenclature:

a notch depth (mm),

b thickness of the specimen (mm),

b_n net specimen thickness ($b_n = b$ if no side grooves are present) (mm),

W width of the specimen (mm),

b_0 $W - a$ (mm), un-notched part of the specimen,

E tangent modulus (MPa),

G_{Ic} fracture energy (J/m^2),

G_{el} elastic component of G_{Ic},

G_{pl} plastic component of G_{Ic},

K_{Ic} fracture toughness (Pa.m$^{1/2}$),

L span between beam supports (mm),

m slope of the tangent of the elastic region of the load vs deflection curve (N/mm),

P_{fail} applied failure load (N),

U area under the load vs displacement curve, between zero and the crack initiation load, (J),

Δ_v vertical displacement of the ITT test specimen (mm),

t thickness of the ITT test specimen (mm),

$\dot{\varepsilon}_{max}$ maximum strain rate (s^{-1})

$\dot{\delta}_{max}$ maximum test rate (mm/s),

δ_{sep} critical separation distance (mm),

σ_{max} tensile strength (MPa),

ν Poisson's ratio.

1. Introduction

Fatigue cracking has long been considered to be a major source of failure in asphalt pavements. Once a crack is initiated in a small area in the pavement, its bearing capacity is decreased and the surrounding undamaged sections of the pavement must carry more load, increasing the potential for crack propagation. In order to predict pavement performance, and its associated service life, a sound understanding of crack initiation mechanisms and crack growth is essential. To characterise the crack resistance of a bituminous mix it is necessary to understand how and where cracks will initiate and subsequently grow to failure. Hartman and Gilchrist [1] studied the process of asphalt pavement cracking through experimental investigations and successfully characterised fatigue behaviour (crack propagation) of two bituminous mixtures by applying a Linear Elastic Fracture Mechanics (LEFM) modelling approach. However, they found that LEFM underestimates the extent of damage that occurs in bituminous materials as LEFM does not consider visco-elastic properties of bituminous materials. Recently Soares et al. [2] have presented a new model based on LEFM theory which considers material visco-elastic behaviour. They adopted a Cohesive Zone (CZ) model within a Finite Element (FE) code to simulate crack growth in an asphalt mix submitted to indirect tensile loading. In contrast to conventional fracture mechanics models, which are based on pre-existing cracks in a body, CZ modelling provides a means of predicting initiation and evolution of a crack in homogenous un-cracked materials until full fracture [3]. Georgiou et al. [4] and Chen et al. [5] illustrated that use of a commercial finite element code (e.g. ABAQUS) and CZ method in fracture analysis can cause significant numerical instabilities. Therefore, in order to

ensure greater numerical stability an open source Finite Volume (FV) code, OpenFOAM [6] was chosen as a suitable alternative. FV method is well known in computational fluid dynamics and has recently emerged as a powerful tool in solving dynamic stress analysis problems [7-10].

Cohesive zone modelling was pioneered by Barenblatt [11] who developed the concept of a cohesive zone to study perfectly brittle materials. Later, Dugdale [12] used the cohesive process zone concept to study materials exhibiting plasticity. Hillerborg et al. [13] successfully extended the cohesive zone concept to study nonlinear fracture processes in concrete. In the last decade or so, the popularity of the CZ concept has increased. The concept has been used to simulate fracture under static and dynamic loading conditions in a number of materials including bituminous materials [14-16], polymers [17-19], metals [20], ceramics [21], composite materials [22,23] and adhesive joints [4,24,25].

The CZ model is usually described using two parameters: fracture energy, *GIc*, and either the maximum cohesive strength, max, or the critical separation distance, sep. In the original cohesive zone concept, Barenblatt [26] defined the maximum predefined stress for mode I crack initiation, as the theoretical strength, max, which is usually several orders of magnitude higher than the actual strength of a solid (often taken as *E*/10, where *E* is Young's modulus). Furthermore, the original Barenblatt/Dugdale CZ model or traction-separation law is initially rigid. From the instant when the normal tractions on cohesive surfaces reach the cohesive strength, max, the cohesive surfaces behave according to the traction-separation law which prescribes the nature by which cohesive surfaces separate from each other. Damage progresses until the separation reaches its critical value sep. At this stage, the material is in a traction free state and is considered to be fractured.

According to Hillerborg [27] the critical mode I energy release rate, G_{Ic} can be computed as:

$$G_{Ic} = \int_0^{\delta_{sep}} \sigma d\delta \qquad (1)$$

Where, σ is the traction acting between the separating surfaces and δ is the separation distance between them.

Williams and Hadavinia [28] stated that the shape of the CZ curve is generally believed to be unimportant to the material separation behaviour, although a wide range of CZ shapes have been used for modelling the fracture of different materials. Furthermore *GIc* is considered to be the main parameter governing both the material surface decohesion and the associated fracture

process. However, there is a number of papers where a strong influence of the shape of the traction-separation law is demonstrated [29-33].

This paper investigates the applicability of the combined cohesive zone within finite volume model in assessing the behaviour of a bituminous mix subjected to indirect tensile loading. The mode I Dugdale CZ model was used to describe material separation behaviour. The material is modelled as a linear elastic – ideal plastic material by adopting the von Mises criterion and Prandtl-Reuss flow rule [34]. Rate dependent material properties and CZ material parameters are independently characterised from experimental procedures. The influence of the shape of the traction separation law was not considered in this paper.

2. Material

The objective in designing the mortar mix in the present research was to reproduce mortar mix proportions as they exist in a typical binder course mix [35-38]. The binder course mortar mix proportions were calculated using only constitutive materials passing through a 6.3mm sieve size, namely sand and Crushed Rock Fines (CRF). The composition of the binder course mix design is listed in Table 1.

Table 1 Aggregate proportion design for 20mm binder course mix.

Aggregate	% Aggregate in Mix
20 (mm)	31
14 (mm)	12
10 (mm)	18
Sand	12
CRF	27

Table 2 illustrates the proportion of various solid components and air voids in the binder course mortar mix. The data presented in Table 2 illustrates an increase in added binder content in the mortar mix in comparison to the 4.5% used in the binder course mix. This occurs as a result of the increase in the surface area of the aggregates in the mortar mix. The mortar mix contains only fine aggregate, which has a greater surface area than a mix containing large aggregates. In order to ensure the retention of the same aggregate binder film thickness, a greater percentage of binder must be added to the mortar mix. By gauging the exact volumetric composition of the original mix, it was determined that the air voids in the mortar mix would be 12%, as indicated in Table 2, and

the target density would be 2.092g/cm^3. In order to gauge the exact void content for the mortar mix, a compaction test was conducted using the gyratory compaction method [39].

Table 2 Mortar mix design. Percentage content of solids is given by weight.

Mix Constituent	% Content in Mix
Sand	27.5
CRF	61.8
Binder	10.7
Air void content = 12%	

3. Experimental procedures

The uniaxial tensile test and three-point bend (3PB) test methods were employed in order to determine material stress-strain curves and the CZ parameters (G_{Ic}, σ_{max}) [40-43]. These and similar methods were used by Soares et al. [2], Song et al. [14], Kim et al. [15] and De Souza et al. [16] for the determination of asphalt pavement parameters.

3.1 Determination of stress – strain curves and CZ Strength (σmax)

The uniaxial tensile test was employed in order to determine the binder course material stress-strain curves and CZ strength (σ_{max}). In this work, it is assumed that CZ strength (σ_{max}) is equal to Ultimate Tensile Strength (UTS) of the material at a given strain rate. Similar assumption was used by a number of authors. For example, numerical predictions were found to closely fit experimental results in fracture of adhesive joints when σ_{max} in taken as UTS [4, 24, 25]. A uniaxial tensile test design procedure devised by Dunhill et al. [44] was employed in this study. The tensile test specimen geometry is presented in Figure 1(a). A special compaction method was designed to manufacture the tensile specimen. The compaction mould was constructed by incorporating two side inserts into the standard concrete compaction mould [45].

Figure 1(b) illustrates the uniaxial tensile test system set up. The test specimens were fastened by applying a combination of marine Epiglass HT 9000 epoxy resin and hardener to the two custom-made loading plates. In order to minimise the effects of bending on the loading plates, the plates were constructed from high stiffness tool steel (E ≈ 207GPa). The uniaxial tension tests were conducted at a room temperature of 20°C at three test rates: 1, 0.1 and 0.01mm/s, with four repeats per test condition.

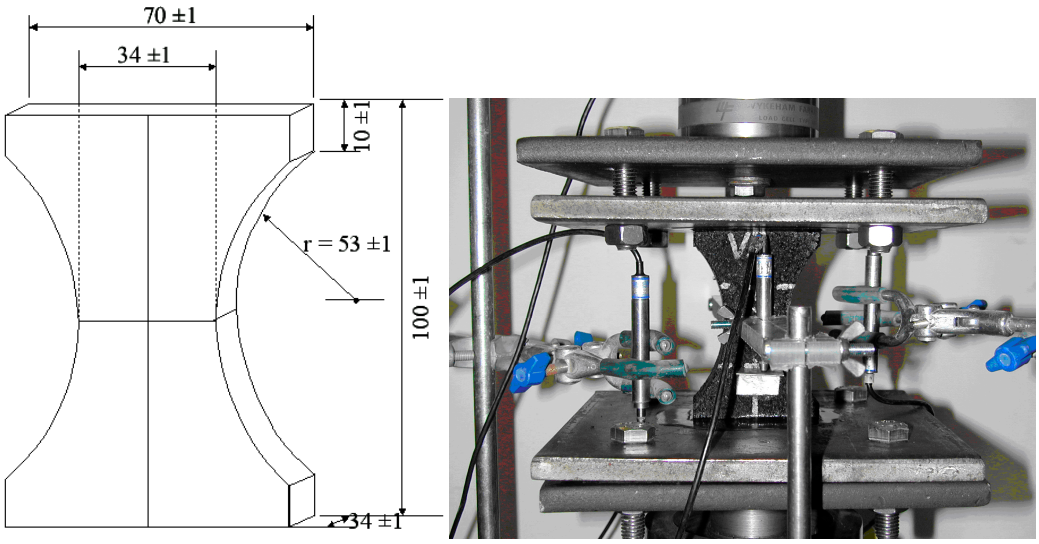

a) b)

Figure 1 (a) Tensile test specimen (dimensions are given in mm). (b) General view of uniaxial tensile test system set-up.

The results presented in Figure 2 show the load-displacement response of the mortar mix materials subjected to uniaxial tensile loading conditions. The strain-rate sensitivity of the material resulting from the different applied test rate results is clearly evident in Figure 2. In each case material failure occurs in a very gradual, ductile manner. Figure 3 illustrates the material stress strain response. The irregular shape of the test specimen gives rise to an irregular strain distribution throughout the specimen. Such irregularities cause greater than average strain values at certain sections within the specimen. The highest strains are expected to occur at the mid plane of the specimen. Knowing the specimen geometry, it is possible to determine a strain concentration factor to calculate the exact strain level at the middle of the test specimen [45]. For this research the strain concentration factor was calculated as 1.35, i.e. the strain in the middle of the test specimen is 35% greater than the average strain. Where the average strain is defined as the ratio of the displacement over the gauge length of the test specimen. The Young's modulus, *E*, of the binder course mortar mixtures, under various loading conditions, were determined using a linear regression analysis performed on initial elastic part of the uniaxial tensile test data, (see Table 3 for details of parameters). The test results demonstrate that increasing the test rates enabled the material to withstand higher stress levels.

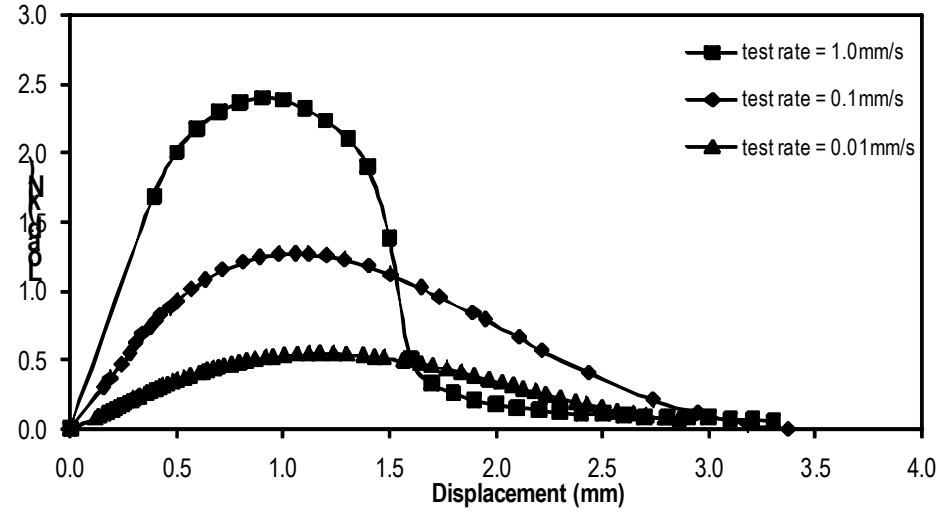

Figure 2 Uniaxial tensile test load vs displacement results for BC mortar mix at 20°C.

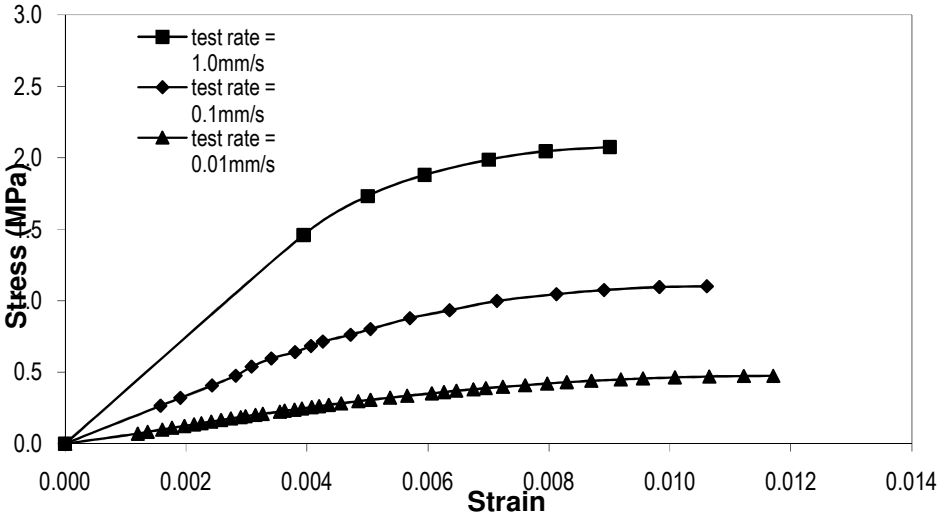

Figure 3 Uniaxial tensile test stress vs strain, results for BC mortar mix at 20°C.

Table 3 Measurements of mortar mix material properties subjected to the uniaxial tensile loading, for different test rates.

Test rate (mm/s)	Max strain rate (s^{-1})	Young's Modulus (MPa)	Tensile strength (N/mm^2)
1.0	1.35 E-2	274.3	2.07
0.1	1.35 E-3	124.8	1.10
0.01	1.35 E-4	46.0	0.47

3.2 Determination of CZ Fracture Energy (G_{Ic})

The 3PB test method, as described in ASTM E 1820 [46], was employed in order to determine the binder course mortar mix fracture energy (G_{Ic}). Single Edge Notch Bend test specimens (length = 260, width = 40 and thickness = 20mm) were machined from the cured slabs. Slab specimens were produced with dimensions of 305mm long, 305mm wide and 20mm high using the standard Coopers Research Technology Roller Compactor [47]. The underside of the test specimens, which are exposed to the maximum tensile stress, were machined in order to ensure a good quality surface with uniform initial flaw size and to reduce the potential scatter in the results. The specimens were cut using a standard bench circular saw with a diamond tipped blade. The specimens were water cooled during machining and were subsequently dried for 24 hours. A notch and side grooves were cut at the centreline of the beam specimens using a standard milling machine. The notch depth and width were 8mm and 2mm, respectively. The depth and width of the side groves were both 2mm. A schematic representation of the test system and test sample is presented in Figure 4.

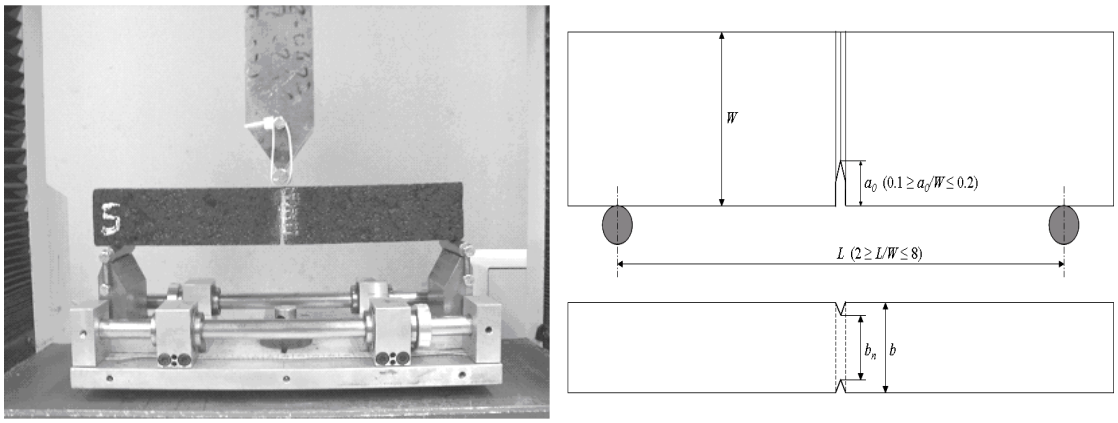

Figure 4 (a) View of 3PB loading fixture. Specimen length and height were 260mm and 40mm, respectively. (b) Schematic representation of a SENB test specimen with side grooves. (Top) Front view. (Bottom) Top View. Dimensions used in this work L = 240mm, *W* = 40mm, b = 20mm, b_n = 16mm, a_0 = 8mm.

The three-point bend tests were conducted on a Tinius Olsen H50kN uniaxial testing frame. In order to avoid embedment of the loading and support fixtures into the test specimen during the test, a set of cylindrical pins were added to the loading and support fixture at the point of the contact with the test specimen (Figure 4(a)). An environmental chamber was used to pre-

condition the specimens at a temperature of 20°C, for 24 hours prior to testing. The testing process involved loading the specimens at constant pre-set displacement controlled test rates of 1.0, 0.1, 0.01 mm/s until failure. Tests were repeated four times per test condition good repeatability was found. Typical load vs. deflection curves for the binder course mortar mix are given in Figure 5.

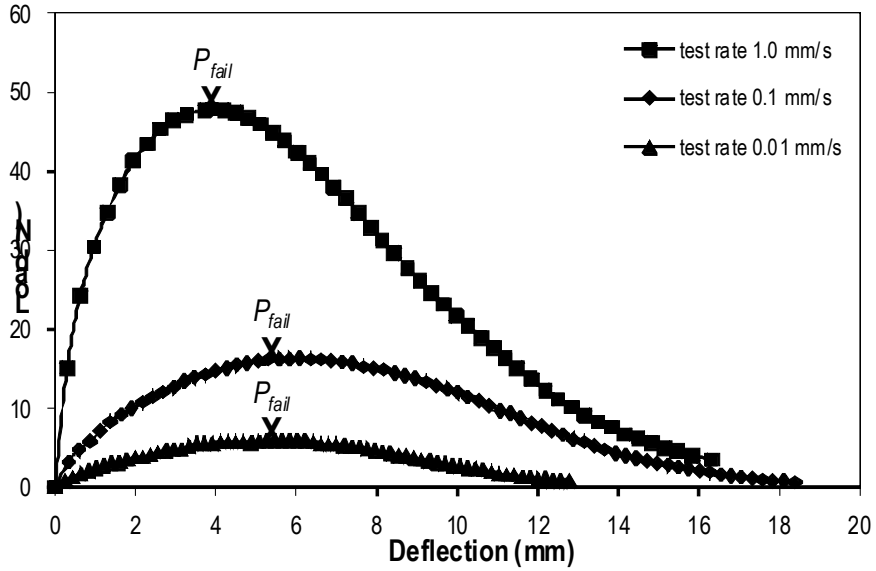

Figure 5 Typical 3PBT load vs deflection plots for BC mortar mix at 20°C at varying test rates.

Following ASTM E 1820 [46], fracture toughness was determined from the specimen dimensions and the load at failure according to the following relationship:

$$K_{Ic} = \frac{P_{fail} L}{\sqrt{b b_n} W^{3/2}} f(x) \qquad (2)$$

where: b = thickness of the specimen (mm),

b_n = net specimen thickness ($b_n = b$ if no side grooves are present) (mm),

W = width of the specimen (mm),

$$f(x) = \left(\frac{3x^{1/2}\{1.99 - x(1-x)[2.15 - 3.93x + 2.7x^2]\}}{2(1+2x)(1-x)^{3/2}} \right)$$

x = a/W

For granular based materials such as asphalt, crack growth is accompanied by aggregate interlocking, micro-cracking and inelastic deformations. These mechanisms give rise to nonlinear

deformations, plasticity and micro-cracking. Therefore, for ductile materials such as asphalt the fracture energy is partitioned into elastic and plastic components and calculated as [46]:

$$G_{Ic} = G_{el} + G_{pl} \quad (3)$$

Elastic fracture energy values were determined from the calculated fracture toughness, experimentally measured modulus, *E*, and Poisson's ratio, v. In the current work Poisson's ratio is estimated as 0.4.

$$G_{el} = \frac{K_{Ic}^2(1-\nu^2)}{E} \approx 0.84\frac{K_{Ic}^2}{E} \quad (4)$$

The plastic constituent for total fracture energy, G_{pl}, is calculated as:

$$G_{pl} = \frac{2U}{b_n b_0} \quad (5)$$

where: b_0 = $W - a$,

U = area under the load vs displacement curve, between zero and the crack initiation load (P_{fail}), (J).

a = notch depth (mm),

Table 4 summarises the calculated fracture energy values from three-point bend tests conducted at three different test rates with corresponding strain rates.

Table 4 Summary of the fracture energy, G_{Ic}, measurements at different test rates.

Test rate (mm/s)	**Max strain rate (s^{-1})**	**Fracture energy, (J/m^2)**		
		Elastic, G_{el}	**Plastic, G_{pl}**	**Total, G_{Ic}**
1.0	3.33 E-3	28.8	549.7	578.5
0.1	3.33 E-4	6.6	281.8	288.4
0.01	3.33 E-5	2.5	85.2	87.7

3.3 Indirect Tensile Test (ITT)

The ITT were conducted following the procedure outlined in the European Standard: EN 12697: Part 23 [48]. The basic procedure of the ITT is to apply a vertical compressive load to a cylindrical specimen. The load is distributed over the thickness of the specimen through two loading strips at the top and bottom, as indicated in Figure 6(a). The contact surfaces of the loading strips are curved and have a radius equal to that of the specimen to ensure full contact over the entire mating area. Linear Variable Displacement Transducers (LVDTs) are used to measure the response of the specimen: two in the horizontal direction along the diameter and two in the vertical

direction. All specimens tested were 100mm in diameter and 70mm thick, with a 10mm wide loading strip. This combination of specimen geometry and boundary conditions induces tensile and compressive stress along both the vertical and horizontal diameters, as indicated in Figure 6(b). The tensile stresses, which develop perpendicularly to the direction of the load, are of relatively constant value over a large portion of the vertical diameter. This would be expected to cause failure of the specimen by splitting along the vertical diameter, as indicated in Figure 6(a).

Although the stress state within an ITT specimen is complex, critical stresses and strains are readily computed from equations based on linear elasticity theory. It is assumed that the material is homogeneous and isotropic. The loading strips are simplified as line loads, as illustrated in Figure 6(b). Hartman [49] summarised the solutions for the linear elastic stress analysis of an ITT test specimen. On the points along the vertical diameter the maximum stresses in the x and y directions are as follows:

$$\sigma_{x\max} = \frac{2P}{\pi.d.t} \qquad (6)$$

$$\sigma_{y\max} = \frac{-6P}{\pi.d.t} \qquad (7)$$

where: $\sigma_{x\max}$ = maximum stress component in the x direction on the vertical line (Pa),

$\sigma_{y\max}$ = maximum stress component in the y direction on the vertical line (Pa),

P = applied vertical load (N),

d = diameter of the specimen (mm),

t = thickness of the specimen (mm).

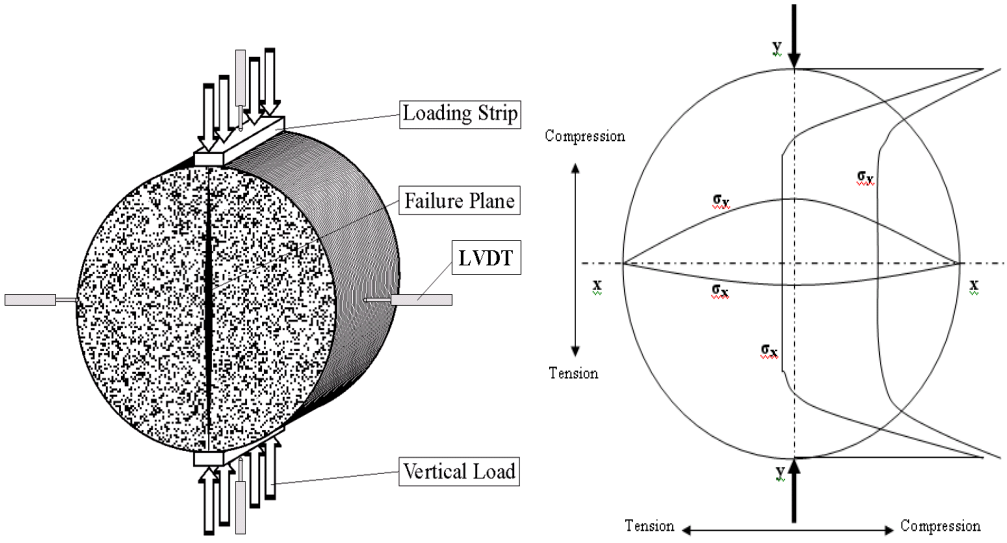

a) b)

Figure 6 Indirect Tensile Test (ITT): (a) Indirect tensile loading, (b) Stress distribution in an indirect tensile test specimen [56].

By applying Hooke's Law the critical/maximum value for the tensile strain, occurring in the centre of the specimen on the x-plane, can be calculated:

$$\varepsilon_{x\max} = \frac{\sigma_{x\max}}{E} - \frac{\upsilon.\sigma_{y\max}}{E} \quad (8)$$

Substituting Eqs (6) and (7) into (8) leads to:

$$\varepsilon_{x\max} = \frac{\sigma_{x\max}.(1+3\upsilon)}{E} \quad (9)$$

It is also possible to determine the material stiffness from the vertical deformation, Δ_v [50]:

$$E = 3.59\frac{P}{\Delta_V.t} \quad (10)$$

Figure 7 and Table 5 illustrate the ITT results of the binder course mortar mix subjected to three different test rates; 1.0, 0.1 and 0.01mm/s. The results clearly indicate material sensitivity to the applied test rate.

Table 5 Measurements of mortar mix material properties subjected to the ITT loading for different test rates.

Test rate (mm/s)	**Max strain rate (s^{-1})**	**Max Load, P, (kN)**	**Youngs Modulus, E, (MPa)**	**Poissons ratio, υ**	**Max vertical deflection (mm)**
1.0	3.9 E-3	7.3	154	0.4	3.8
0.1	3.9 E-4	3.2	62	0.4	3.5
0.01	3.9 E-5	1.3	46	0.4	2.8

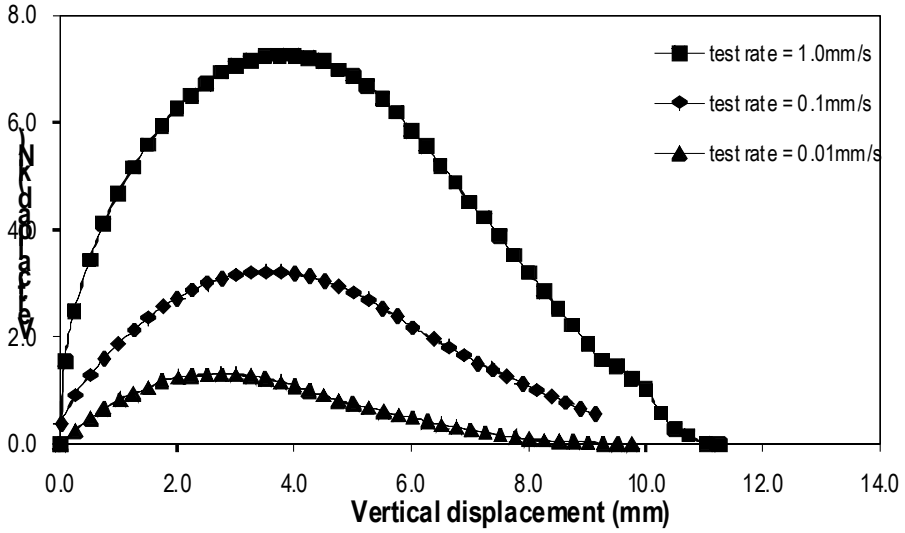

Figure 7 Indirect Tensile Test (ITT) results for BC mortar mix at 20°C.

3.4 Determination of the material and CZ parameters as a function strain rate

The same applied test rate in the 3PB test, uniaxial tensile test and ITT test does not result in the same strain rate. Hence the strain rates must be determined for each test and employed to obtain corresponding rate dependent material properties. The strain rates were determined for each test, and by interpolation between these strain rates, the cohesive strength, σ_{max}, yield stress, σ_{yield} and Young's modulus, E, were obtained as functions of strain rate. The strain rates for 3PB tests were calculated using the following equation [51]:

$$\dot{\varepsilon}_{\max} = \dot{\delta}_{\max} \frac{6b_0}{L^2} \tag{11}$$

where: $\dot{\varepsilon}_{\max}$ = maximum strain rate (s^{-1})

$\dot{\delta}_{\max}$ = maximum test rate (mm/s),

L = span between 3PB test beam supports (mm),

b_0 = $W - a$ (mm).

The tensile test strain rate was determined using the following equation [52, 53]:

$$\dot{\varepsilon}_{\max} = \left(\frac{\dot{\delta}_{\max}}{h} \right) \times K_t \tag{12}$$

where: h = specimen height (mm),

K_t = stress/strain concentration factor, (K_t = 1.35).

The inclusion of the stress/strain concentration factor, K_t, is required due to the irregular cross section of the tensile specimens, as discussed in section 3.1. The irregular cross section gives rise

to irregularities in stress/strain distribution throughout the specimen. The highest strains are expected to occur at the middle of the specimen. Using specimen geometry, and the ratio between the smallest and the largest width, the value of the stress/strain concentration factor, K_t, found to be 1.35 [45, 53].

The strain rate for the ITT test was calculated using the following equation [48, 49]:

$$\dot{\varepsilon} = \frac{\varepsilon_{x\max}}{\Delta_V / \dot{\delta}_{\max}} \qquad (13)$$

Table 3, Table **4** and Table **5**, present calculated strain rates for uniaxial tensile, three-point bend and indirect tensile tests respectively at the same test rates. Material and CZ parameters required for the numerical simulations of ITT tests were obtained as a function of strain rate by interpolating/extrapolating experimentally measured data from the uniaxial tensile and 3PB tests.

The cohesive strength , σ_{max}, and Young's modulus, E, for corresponding ITT strain rates were obtained using the uniaxial test results as a function of strain rates. The values of σ_{max} and E were interpolated and extrapolated as shown in Figure 8 and Figure **9**, respectively. The approximation functions in the semi-logarithmic graphs are second-order polynomials passing through all three experimental data points. Thus, the values of σ_{max} and E were interpolated for 1mm/s and 0.1mm/s test rate. However, due to lack of experimental data at lower rates, the value for the 0.01mm/s test rate was extrapolated. The values of σ_{max} and E at the corresponding ITT rates are also summarised in Table 6.

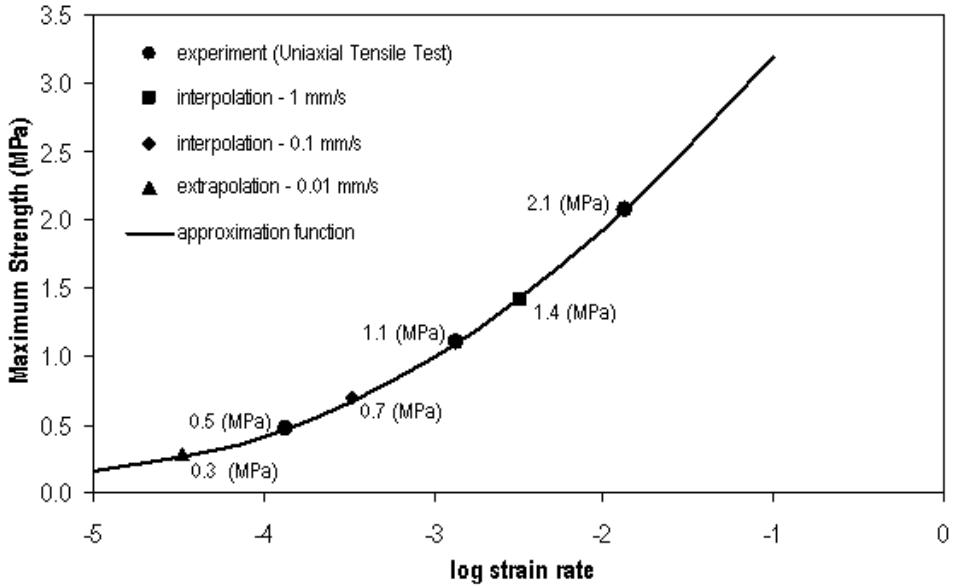

Figure 8 Interpolated and extrapolated cohesive, σ_{max}.

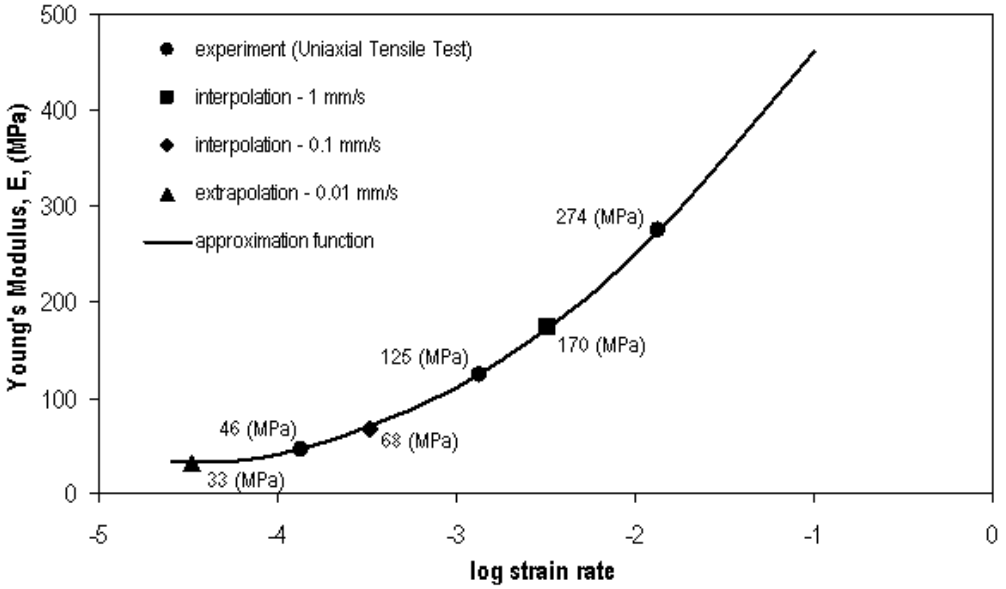

Figure 9 Interpolated and extrapolated Young's Modulus, E.

Table 6 CZ and material parameters, i.e. input data for ITT simulations.

Test rate (mm/s)	**Modulus (MPa)**	**Poissons ratio, ν**	**Yield stress, (MPa, numerical)**	**Yield stress, (MPa) (extrapolated)**	**CZ stress, σ_{max} (MPa)**	**Fracture energy, G_{Ic} (J/m^2)**
1.0	170	0.4	2.57	2.87	1.4	578.5
0.1	68	0.4	1.15	1.35	0.7	288.4
0.01	33	0.4	0.46	0.50	0.3	87.7

Table 4 and Table **5** illustrate that strain rates for ITT and 3PB tests are similar, for a given test rate. Hence, the fracture energy values were taken directly from the 3PB test results and employed in the simulation of the ITT for the three corresponding test rates. Table 6 summarises the fracture energy, G_{Ic}, values as a function of strain rate used in ITT test simulations.

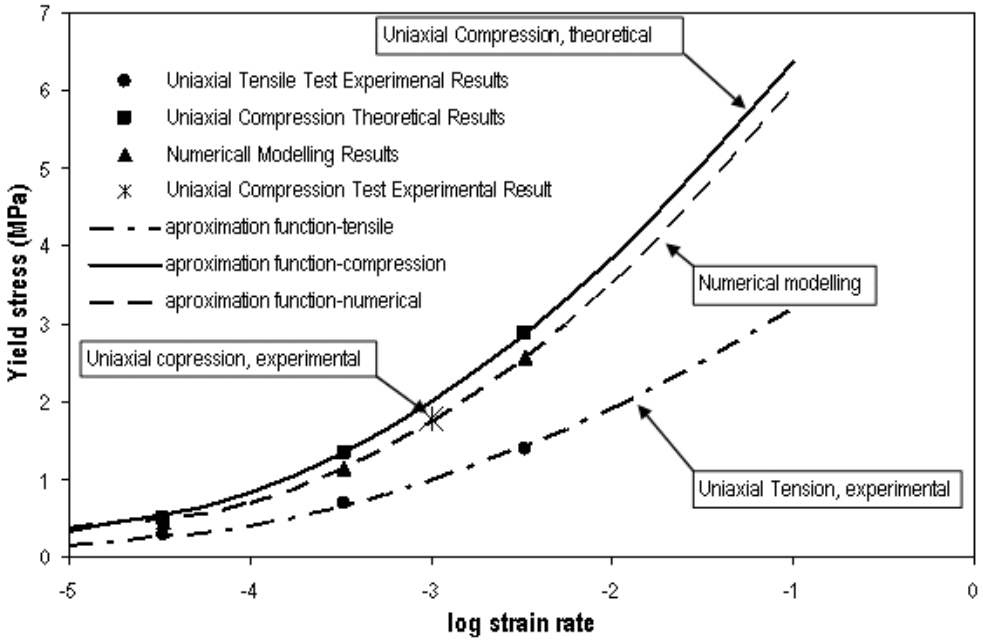

Figure 10 Variation of yield stress with strain rate as measured experimentally and predicted numerically. Results presented on the numerical modelling curve were used as σ_{yield} parameters in ITT model.

Finally, to account for plastic deformation in the simulations of ITT (the material was modelled as linear elastic – ideally plastic) the values of yield stress, σ_{yield}, were required at different strain rates. However, due to a lack of compressive experimental data the appropriate yield stress values in compression were obtained by using the uniaxial tensile yield stress data at the appropriate strain rate, see Figure 10. Previously published work [44] shows that the yield stress in compression for the bituminous material is approximately twice the yield stress in tension. Hence for the numerical modelling of the ITT test, yield stress in compression at a given strain rate is used as twice the yield stress from a uniaxial tensile test at the corresponding strain rate (see Figure 10). Independent numerical modelling of ITT test also gave similar values for the yield stress in compression; Figure 10 illustrates best fit values. In the simulations, the value of the σ_{yield} for a given test rate was varied until a good fit between numerical and experimental load vs. displacement curves was achieved. In order to verify the theoretical and numerical compression yield stress results, a compression test was performed. A set of cylindrical test specimens, 100mm in height and 50mm in diameter, were cored from the slabs, 305mm in length, 305mm in width and 100mm in height, as illustrated in Figure 11. The uniaxial compression tests were conducted at a room temperature of 20°C at a test rate, of 0.1mm/s, and were repeated on four test specimens.

Figure 11 illustrates the compressive load fixture set up. A friction reduction protocol, based on silicone and graphite lubricant, was used to minimise the lateral confinement of the specimens resulting from friction between the plates and the specimen ends. The strain rate for the compression test was calculated as:

$$\dot{\varepsilon}_{\max} = \left(\frac{\dot{\delta}_{\max}}{h} \right) \tag{14}$$

Figure 11 Left; coring the test specimens from the slab. Right; compressive load fixture

Due to the specimen's geometric uniformity, the stress/strain concentration factor, K_t, was equal to unity. The calculated strain rate was $0.001s^{-1}$ and the yield stress was 1.773MPa for the corresponding test rate of 0.1mm/s. Figure 10 illustrates that the experimentally determined compressive stress is very close to the theoretical compressive yield stress, thus validating the theoretical and numerical results.

4 Numerical Model

4.1 Introduction

Two numerical methods have been reported for implementing CZ models for the analysis of asphalt fracture, namely the discrete element method (DEM) and the finite element method (FEM). Kim et al. [15] used the DEM to implement a CZ model in order to simulate failure of asphalt laboratory test specimens. The FEM has been more widely used in the analysis of asphalt pavement fracture, most recently by Soares et al. [2], Song et al. [14] and De Souza et al. [16]. The present work follows that of Ivanković et al. [3], Georgiou et al. [4], Cooper et al. [24] and Karač et al. [25], where the finite volume (FV) method was employed with a CZ model to analyse fracture of ductile polymers and adhesives. They employed a transient analysis for an apparently static problem to avoid numerical instabilities caused by rapid separation of cohesive surfaces.

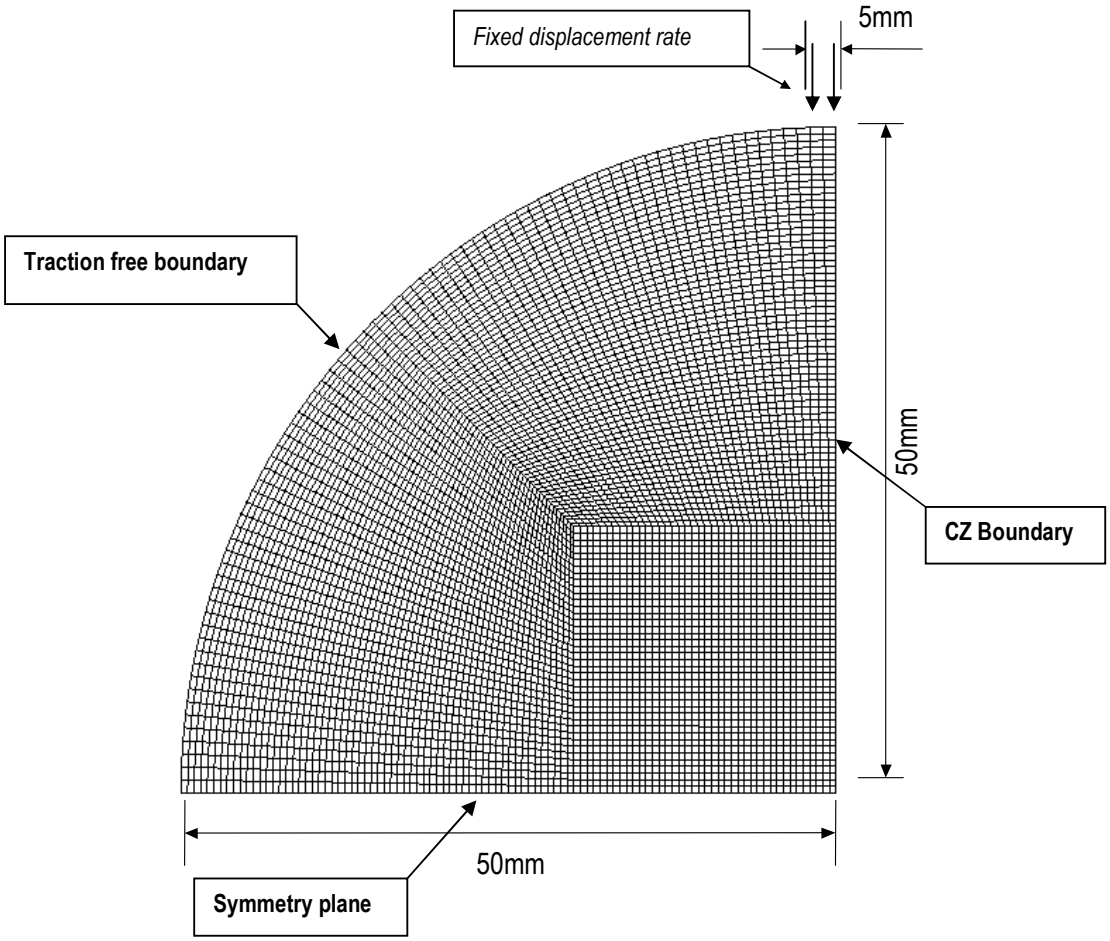

Figure 12. Schematic representation of the ITT geometry in finite volume.

Similar procedures were also employed here for numerical simulation of a binder course mortar mix subjected to indirect quasi-static tensile loading. In this study the material was modelled as linear elastic – ideally plastic, assuming conventional J2 flow theory which is based on von Mises yiels criterion and Prandtl-Reuss flow rule [34]. The code was implemented in the OpenFOAM software, a C++ library for continuum mechanics [6]. A fully implicit time stepping algorithm was employed in the analysis, guaranteeing unconditional stability.

4.2 Modelling of ITT

A schematic illustration of the FV mesh representing the ITT test specimen and applied boundary conditions is given in

Figure 12. Due to symmetry, only a quarter of the domain was modelled. The model was meshed using 6400 three-dimensional hexahedral cells with maximum cell dimensions of 0.5mm. The displacement rate corresponding to the test rate was applied directly at the top of the specimen model over 5mm width, simulating constant test rates of 1.0mm/s, 0.1mm/s and 0.01mm/s. The Dugdale CZ was applied at the right edge of the model. The bottom edge was modelled as a plane of symmetry, whereas the outer surface was traction free. The front and back surfaces were symmetry planes to account for plane strain condition. The time step applied was 0.05 s, 0.5 s and 5 s for the 1 mm/s, 0.1 mm/s and 0.01 mm/s simulations, respectively.

The CZ Dugdale traction law was employed to describe the traction separation behaviour of the binder course mortar material along the anticipated crack path. In the beginning of the simulation, the cohesive surface was modelled as a symmetry plane, since the Dugdale traction-separation law is initially rigid. Once the stress level reached its maximum value, σ_{max}, the cohesive surface behaviour was governed by CZ and material became irreversibly damaged. Increasing load or displacement, resulted in increased separation of the cohesive surface which eventually reached its critical value, δ_{sep}, the critical crack opening displacement. At this stage the material was fractured and the cohesive surfaces became stress free (i.e., zero traction). The work done by the cohesive forces is equal to the fracture energy, G_{Ic}. Material and CZ parameters used in numerical simulations of ITT tests were obtained experimentally by uniaxial tensile (Young's modulus, E, and CZ maximum strength value, σ_{max}), and 3PB tests (fracture energy, G_{Ic}), as discussed in Section 3.

4.3 Modelling results

Figure 13 and Figure **14** compare the simulated material response with the experimental ITT test results when using two different sets of Young's modulus and yield stress values. Figure 13 presents the simulated material response using the interpolated and extrapolated values from the uniaxial tensile test results (c.f. Table 6 for actual values). Figure 14, on the other hand, presents the simulated response using the Young's modulus value as obtained directly from the ITT test (c.f.Table 5) and the numerical best fit value for yield stress (c.f. Table 6). The results shown in both Figure 13 and Figure **14** demonstrate a good correlation between the predicted and measured load-displacement responses for the loading portion of the response for all three test rates. The numerical simulations accurately predict the location and load (time) at which crack initiation occurs. Consequently, a reasonably accurate value of the indirect tensile strength (ITS) of

the material is provided by the simulations at each of the test rates. Small differences between the numerical predictions of Figure 13 and Figure **14** are due to the uncertainties involved in obtaining material parameters for different test rates. Also, interpolation and extrapolation was based on an average strain rate values while the actual strain rates are not uniform within the specimens.

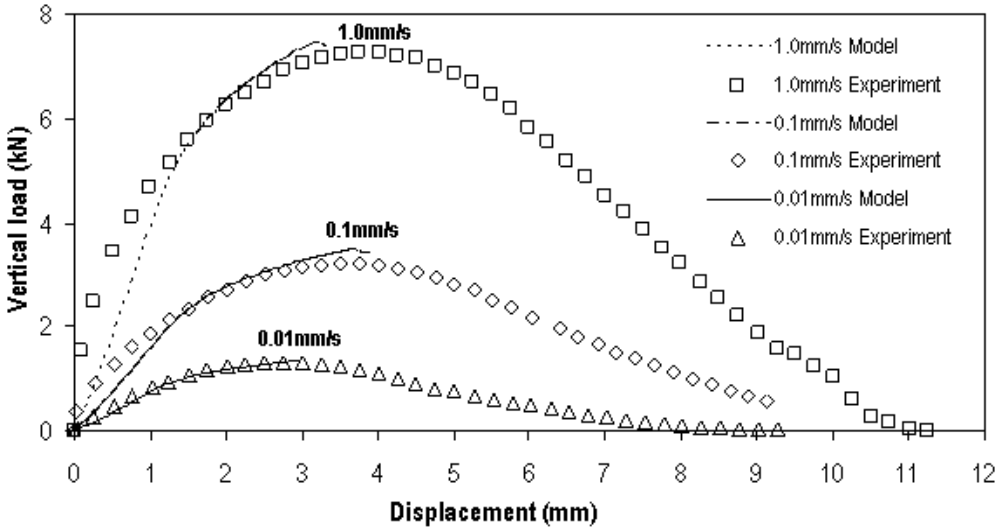

Figure 13 Comparison of CZ+FV modelling predictions and experimental results for different test rates, (symbols correspond to experimental results and continuous lines to 2D FV model results).

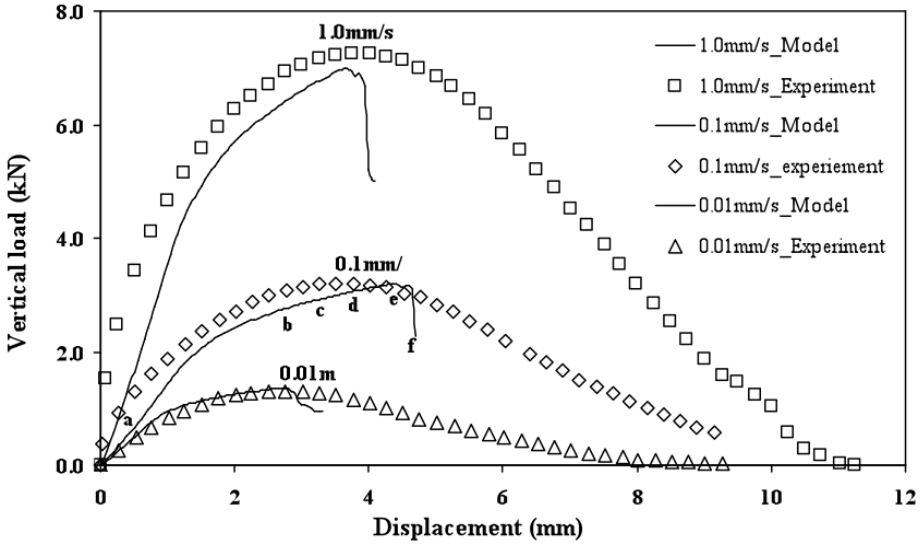

Figure 14 Comparison of CZ+FV modelling predictions and experimental results for different test rates, (symbols correspond to experimental results and continuous lines to 2D FV model results). The letter markers in the graph, on the line illustrating 0.1mm/s modelling results, correspond to the crack propagation stages presented in the Figure 15.

4.4 Discussion

Images illustrated in Figure 15, present a sequence of numerical prediction of ITT sample at different times during loading. The images demonstrate the crack initiation and propagation stages and horizontal stress distribution (σ_{xx}) throughout the specimen model. The images illustrate a high concentration of compressive stress in the region under the loading platens resulting from compressive load applied to the test specimen. A relatively high tensile stress along the centreline can also be observed due to the indirect tensile loading induced onto the test specimen. These results correspond very well with the theoretical stress distribution explained earlier in Section 3.3 and illustrated in Figure 6(b). They also illustrate that crack initiation and propagation, as expected, occur due to the tensile stress close to the centre of the specimen. Following crack initiation, the crack propagates towards the top and the centre of the specimen. Due to the fast crack propagation in all simulations (at all rates) predicted load drops rapidly after the initiation point, as illustrated in Figure 15 and corresponding load response is shown in Figure 14.

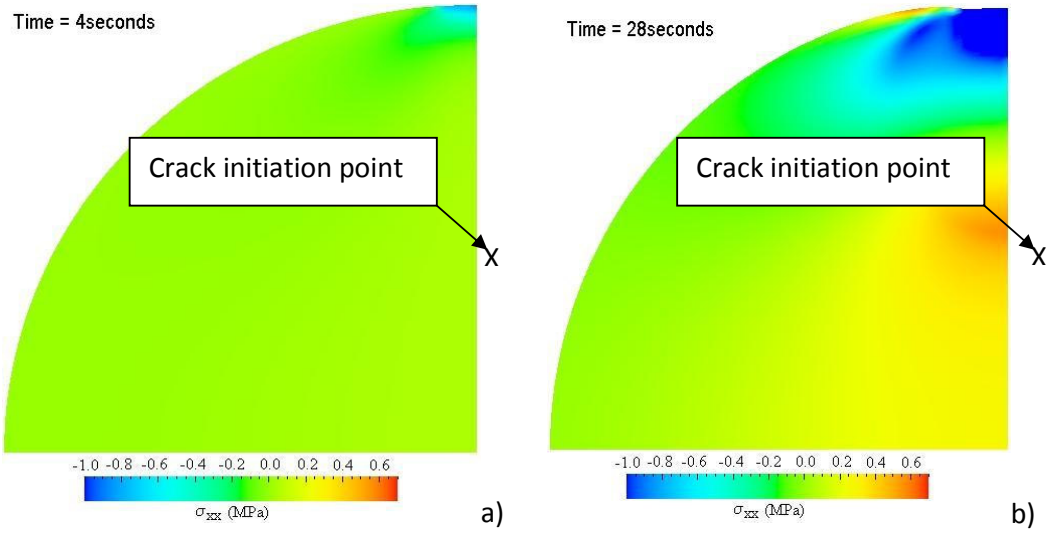

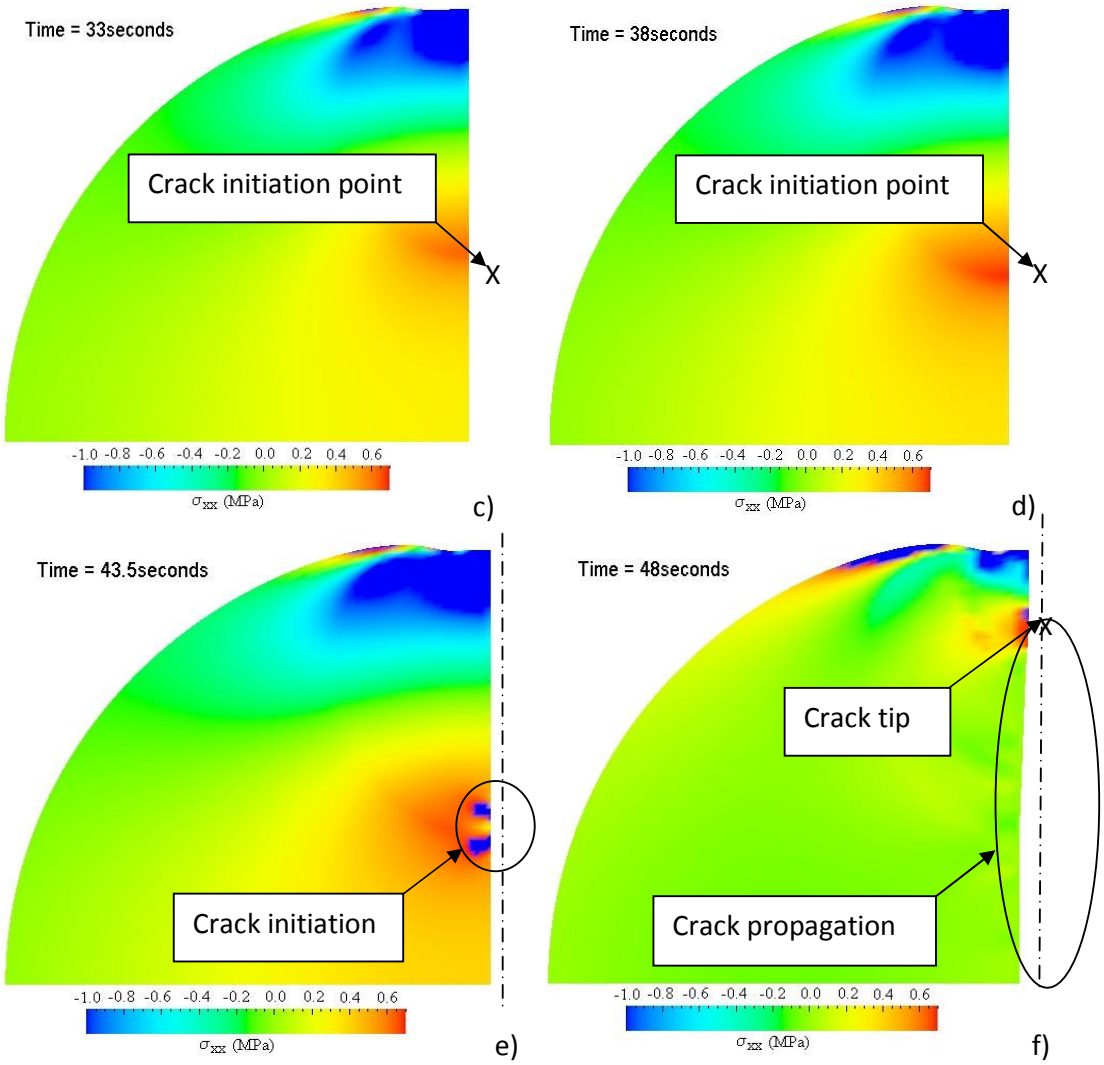

Figure 15 Frame images from the CZ+FV model subjected to 0.1mm/s vertical loading, corresponding to the markers on the 0.1mm/s curve presented in Figure 14.

The model's inability to simulate the softening part of the material response is partly due to the assumption that the specimen will fail via a cracks confined to propagate along the vertical centre line of the specimen. In addition, the simulations were conducted using fixed material and CZ parameters at a given test rate. However, the actual strain rates and corresponding properties vary both with time and position along the crack path. The numerical predictions obtained using fixed rate traction-separation laws and fixed material properties may not be able to accurately simulate the response of bitumen, which is a rate dependent material. Secondly, the constraint level may vary within the specimen. While a high constraint CZ may be appropriate for cells in the vicinity of the crack tip where high lateral constraints exist, it may not be appropriate to describe cells remote from the crack tip where lower constraint conditions prevail. In order to predict the crack growth more accurately it would be necessary to update the traction separation law both in

terms of varying the constraints and strain rate even for the fixed test rate test. Ivanković et.al. [3] reported an improved solution for modelling the softening part of load-displacement by incorporating a rate dependent cohesive zone, while effects of constraint on CZ predictions were widely reported [24, 25, 32, 54]. Models where multiple cracks play an important role were developed by Murphy and Ivanković [17]. They simulated dynamic fracture in polymethylmethacrylate (PMMA) by inserting cohesive cells between the continuum elements. Using this approach, they successfully modelled micro crack branching throughout the sample and found out that branching is responsible for apparent increase in fracture energy. In order to simulate the evolution of cracks subsequent to crack initiation in bituminous materials, further work is necessary to establish rate and constraint dependant CZ models, in addition to using a multiple crack simulation approach.

5. Conclusions

The current code of practice in asphalt pavement mix design [55] is to use a recipe-based approach, with the mix designed to follow an aggregate grading. However, using such an approach demands intensive laboratory investigation of the mix performance, which is both expensive and time consuming. Development of a numerical model, such as presented in this paper, has the potential to allow a rapid and inexpensive assessment of a pavement mix design, leading to an accurate analysis of pavement performance subjected to realistic loading conditions.

This research demonstrated that the Dugdale traction law can successfully predict the mortar mix material loading response when subjected to complex loadings such as indirect tension. The three-point bend (3PB) and uniaxial tensile tests were employed to determine the CZ parameters and material stress-strain curves as a function of strain rate. Numerical results, expressed by load-displacement curves, agree well with experimental data up to the peak load, demonstrating the value of the CZ modelling technique in successfully predicting maximum material strength and the initiation of fracture. Future work will employ a true rate- and constraint-dependent CZ model and a multiple crack simulation approach, in order to capture and predict the complete softening behaviour, and as such could be used to simulate the entire fracture process in bituminous materials.

Acknowledgements

The authors wish to thank Mr. Tom Webster, University College Dublin, for his assistance with the laboratory testing, Enterprise Ireland (ATRP\02\413) for providing funding for this research and both Roadstone Dublin Ltd. and Shell Bitumen Ireland for supplying raw materials.

References

[1] Hartman, A.M. and Gilchrist, M.D., 2004, "Evaluating four-point bend fatigue of asphalt mix using image analysis". ASCE Journal of Materials in Civil Engineering, 16 (1), pp. 60-68.

[2] Soares, J.B., Colares de Freitas F.A., Allen D.H., 2003, "Crack modeling of asphaltic mixtures considering heterogeneity of the Material", Journal of Transportation Research Record: Journal of the Transportation Research Board, No. 1832, pp.113–120, National Research Council,Washington, D.C., U.S.A.

[3] Ivanković, A., Pandya, K.C. and Williams, J.G., 2004, "Crack growth predictions in polyethelyne using measured traction – separation curves". Engineering Fracture Mechanics, 71, pp. 657 – 668.

[4] Georgiou, I., Hadavinia, H., Ivankovic, A., Kinloch, A.J., Tropsa, V. and Williams, JG, 2003, "Cohesive zone models and the plastically deforming peel test", Journal of Adhesion, 79 (3), pp. 239-265.

[5] Chen, J.; Cisfield, M.; Kinloch, A.J.; Busso, E.; Matthews, F.L. and Qiu, Y, 1999, "Predicting progressive delamination of composite material specimens via interface elements", Journal of Mechanics of Composite Materials and Structures, Vol. 6, 4, pp. 301-317.

[6] Weller, H.G., Tabor, G., Jasak, H. and Fureby, C., 1998, "A tensorial approach for continuum mechanics using object orientated techniques". Computers in Physics, 12 (6), pp. 620-631. Software available from www.opencfd.co.uk/openfoam.

[7] Versteeg, H. and Malalasera, W., 2007, "An introduction to computational fluid dynamics: The Finite Volume Method", Prentice Hall, 2nd ed. ISBN: 9780131274983.

[8] Stylianou, V. and Ivanković, A., 2002, "Finite Volume Analysis of dynamic fracture phenomena. I. A mode release methodology", Int. Journal of Fracture, Vol. 113, pp. 107-123.

[9] Ivanković, A., 1999, "Finite Volume modelling of dynamic fracture problems" Computer Modelling and Simulation in Engineering, 4, pp. 227-235.

[10] Ivanković, A.; Demirzić, I., Williams, J.G. and Leevens, P.S., 1994, "Application of the Finite Volume method to the analysis of dynamic fracture probems", Int. Journal of Fracture, Vol. 66, pp. 357-371.

[11] Barenblatt, G.I., 1959, “The formation of equilibrium cracks during brittle fracture: general ideas and hypothesis, axially symmetric cracks”, Journal of Applied Mathematics and Mechanics, 23 (1), pp. 622–636. English translation from PMM, 1959, 23, pp. 434–444.

[12] Dugdale, D., 1960, “Yielding of steel sheets containing slits”. Journal of Mechanics and Physics of Solids, 11 (8), pp. 100-104.

[13] Hillerborg, A., Modeer, M. and Petersson, P.E., 1976, “Analysis of crack formation and crack growth in concrete by means of fracture mechanics and finite elements”. Cement and Concrete Research, 6 (6), pp. 773-782.

[14] Song, S.H., Paulino, G.H. and Buttlar, W.G., 2006, “A bilinear cohesive zone model tailored for fracture of asphalt concrete considering viscoelastic bulk material”. Engineering Fracture Mechanics, 73 (18), pp. 2829-2848.

[15] Kim, H., Wagoner, M.P. and Buttlar, W.G., 2006, “Toward realistic heterogeneous fracture modeling of asphalt mixture using disk-shaped compact tension test based on discontinuum approach”. Transport Research Board, 85 Annual Meeting, Paper Number 2975, National Research Council, Washington, D.C., USA.

[16] De Souza, F.V., Soares, J.B., Allen, D.H. and Evangelista, F. Jr., 2004, “Model for predicting damage evaluation in heterogeneous viscoelastic asphaltic mixtures”. Bituminous Paving Mixtures, Transportation Research Record: Journal of the Transportation Research Board, No. 1891, pp. 131-139, National Research Council, Washington, D.C., U.S.A.

[17] Murphy, N. and Ivanković, A., 2005, “The prediction of dynamic fracture evolution in PMMA using a cohesive zone”. Engineering Fracture Mechanics, 72, pp. 861-875.

[18] Rahulkumar, P., Jagota, A., Bennison, S.J. and Saigal, S., 2000, “Cohesive element modeling of viscoelastic fracture: application to peel testing of polymers”. International Journal of Solids and Structures, 37 (13), pp.1873-1897.

[19] Li, H. and Chandra N., 2003, “Analysis of crack growth and crack tip plasticity in ductile materials using cohesive zone models”, International Journal of Plasticity, 19, pp. 849-882.

[20] Siegmund, T. and Brocks, W., 2000, “A numerical study on the correlation between the work of separation and the dissipation rate in ductile fracture.” Engineering Fracture Mechanics, 67 (2), pp. 139-154.

[21] Camacho, G.T. and Ortiz, M., 1996, “Computational modeling of impact damage in brittle materials”. International Journal of Solids and Structure, 33 (20-22), pp. 2899-2938.

[22] Foulk, J.W., Allen, D.H. and Helms, K.L.E., 2000, “Formulation of a three-dimensional cohesive zone model for application to a finite element algorithm”. Computer Methods in Applied Mechanics and Engineering, 183 (1-2), pp. 51-66.

[23] Espinosa, H.D., Dwivedi, S. and Lu, H.C., 2000, “Modeling impact induced delamination of woven fiber reinforced composites with contact/cohesive laws”. Computer Methods in Applied Mechanics and Engineering, 183 (3-4), pp. 259-290.

[24] Cooper, V.; Ivanković, A.; Karač, A.; McAuliffe, D.; Murphy, N. and Tuković, Z., 2010, “The bond gap thickness effect on the fracture toughness of nano-toughened structural epoxy adhesives”, In Proc. of the 33rd Annual Meeting of Adhesion Society, Ed. Anderson, G., Feb 21-24 2010, Daytona Beach, Florida, USA.

[25] Karač, A.; Blackman, B.R.; Cooper, V.; Kinloch, A.J.; Rodriguez Sanchez, S.; Teo, W.S. and Alojz Ivanković, 2010, “Modelling the fracture behaviour of adhesively-bonded joints as a function of test rate”, Submitted for publication in Engineering Fracture Mechanics.

[26] Barenblatt, G.I., 1962, “Mathematical theory of equilibrium cracks in brittle fracture”, Advances in Applied Mechanics, 7, pp. 55-129.

[27] Hillerborg, A., 1985, “The theoretical basis of a method to determine a fracture energy G_F of concrete”. Materials and Structures, 18 (106), pp. 291-296.

[28] Williams, J.G. and Hadavinia, H., 2002, “Elastic and elasto-plastic correction factors for DCB specimens”. Proceedings of the 14th Biannual Conference on Fracture (ECF 14), 8-13th September, Krakow, Poland.

[29] Alfano, G., 2006, “On the influence of the shape of the interface law on the application of cohesive-zone models”. Composites Science and Technology, 66, pp. 723–730.

[30] Volokh, K. Y., 2004, “Comparison between cohesive zone models”. Communications in Numerical Methods in Engineering, 20, pp. 845–856.

[31] Elices, M., Guinea, G. V., Gomez, F. J. and Planas, J., 2002, “The cohesive zone model: advantages, limitations and challenges”. Engineering Fracture Mechanics, 69, pp. 137–163.

[32] Scheider, I. and Brocks, W., 2003, “The effect of the traction separation law on the results of cohesive zone crack propagation analyses”. Key Engineering Materials, 251, pp. 313–318.

[33] Li, H. and Chandra, N., 2003, “Analysis of crack growth and crack tip plasticity in ductile materials using cohesive zone models”. International Journal of Plasticity, 19, pp. 849–882.

[34] Maneeratana, K., 2000, “Development of the finite volume method for non-linear structural applications”, PhD Thesis, Imperial College London, UK.

[35] Owende, P.M., Hartman, A.M., Ward, S.M., Gilchrist, M.D. and O'Mahony, M.J., 2001, "Minimising distress of flexible pavements using variable tire pressure". ASCE Journal of Transportation Engineering, 127 (3), pp. 254-262.

[36] Gilchrist, M.D., Hartman, A.M., Owende, P. and Ward, S.M., 2001, "Full scale accelerated testing of bituminous road pavement mixtures". Key Engineering Materials, 204-205, pp.443-452.

[37] Hartman, A.M., Gilchrist, M.D., Owende, P., Ward, S. and Clancy, F, 2001, "In-situ accelerate testing of bituminous mixtures". International Journal of Road Materials and Pavement Design, 2 (4), pp. 337-357.

[38] Hartman, A.M., Gilchrist, M.D. and Walsh G., 2001, "Effect of mixture compaction on indirect tensile stiffness and fatigue". ASCE Journal of Transportation Engineering, 127 (5), pp. 370-378.

[39] Comité Européen de Normalisation, 1998, "EN 12697: Part 31. Bituminous mixtures. Test methods for hot mix asphalt. Specimen preparation: gyratory compactor", European Committee for Standardization, Brussels.

[40] Hoare, T.R. and Hesp, A.M., 2000, "Low-temperature fracture testing of asphalt binders. Regular and modified systems". Asphalt Binders, Transportation Research Record: Journal of the Transportation Research Board, National Research Council, Washington, D.C., USA, Number 1728, pp. 36-42.

[41] Williams, J.G. and Cawood, M.J., 1990, "European group on fracture: K_c and G_c methods for polymers". Polymer Testing, 9, pp. 15-26.

[42] Rottler. J., Barsky, S. and Robbins, M.O., 2002, "Cracks and crazes: on calculating the macroscopic fracture energy of glassy polymers from molecular simulations". Physical Review Letter 89, (14); Art. No. 148304.

[43] Shet, C. and Chandra, N., 2004, "Effect of the shape of T-□ cohesive zone curves on the fracture response". Mechanics of Advanced Materials and Structures, 11, pp. 249–275.

[44] Dunhill, S.T., Airey, G.D., Collop, A.C. and Scarpas, A., 2006 "Advance constitutive modelling of bituminous material", International Journal of Pavmenet Engineering, 7 (3), pp. 153 – 165.

[45] Tabaković, A., 2007, "The influence of reclaimed asphalt pavement (RAP) on binder course mix performance". PhD Thesis, University College Dublin, Ireland.

[46] American Society for Testing Materials (ASTM), 2006, "E 1820-01: Standard test method for measurement of fracture toughness". Annual Book of ASTM Standards, Philadelphia, PA, USA.

[47] Cooper Research Technology, 2005, (www.cooper.co.uk).

[48] Comité Européen de Normalisation, 1998, “EN 12697: Part 23. Bituminous mixtures. Test methods for hot mix asphalt. Determination of the indirect tensile strength of bituminous mixtures”, European Committee for Standardization, Brussels.

[49] Hartman A.M., 2000, “An experimental investigation into the mechanical performance and structural integrity of bituminous road pavement mixtures under the action of fatigue load conditions”, PhD Thesis, University College Dublin, Ireland.

[50] Fairhurst, C.E., Kosla, N.P. and Kim, Y.R., 1990, “Resilient modulus testing of asphalt specimens in accordance with ASTM D 4123-82”. Proceedings International RILEM Symposium, Paper 28, Editors: Fritz H.W. and Eustacchio, E., RILEM, Cachan Cedex, France.

[51] Urry, S.A. and Turner, P.J., 1981, “Solution of problems in strength of materials and mechanics of solids”. Fourth edition, ISBN 0273015907, Pitman Publishing Ltd., London, UK.

[52] Timoshenko, S. and Young, D.H., 1968, “Elements of strengths of materials”, 5th Edition, Van Nostrand Company Ltd, Toronto, Canada.

[53] Van Valiet, M.R.A., 2000, “Size effect on tensile fracture of concrete and rock”, PhD. Thesis, Technical University Delft, Netherlands.

[54] Seigmund, T. and Brocks, W., 1999, “Predicting work separation and implications to modeling”, Int. Journal of Fracture, Vol. 99, pp.97-116.

[55] British Standard Institution (BSI), 2005, “BS 4987: Part 1. Coated macadam (asphalt concrete) for roads and other paved areas. Specification for constituent materials and for mixtures”, British Standard Institution, London, UK.

[56] Read, J.M., Collop, A.C. and Singleton T., 1997, “Practical Fatigue Characterisation of Bituminous Paving Mixtures”, Proceedings of the Workshop on Performance Related Test Procedures for Bituminous Mixtures, Editors: Hartman, A. and Gilchrist, M., University College Dublin, Dublin, Ireland, pp. 138-177, ISBN 1857485955.